

Critical and geometric properties of magnetic polymers across the globule-coil transition

Kamilla Faizullina, Ilya Pchelintsev, and Evgeni Burovski
HSE University, 101000 Moscow, Russia

We study a lattice model of a single magnetic polymer chain, where Ising spins are located on the sites of a lattice self-avoiding walk in $d = 2$. We consider the regime where both conformations and magnetic degrees of freedom are dynamic, thus the Ising model is defined on a dynamic lattice and conformations generate an annealed disorder. Using Monte Carlo simulations, we characterize the globule-coil and ferromagnet-to-paramagnet transitions, which occur simultaneously at a critical value of the spin-spin coupling. We argue that the transition is continuous—in contrast to $d = 3$ where it is first-order. Our results suggest that at the transition the metric exponent takes the theta-polymer value $\nu = 4/7$ but the crossover exponent $\phi \approx 0.7$, which differs from the expected value for a θ -polymer.

I. INTRODUCTION

A linear polymer in thermal equilibrium in a solvent can be either extended (“swollen”), or collapsed into a dense globule, depending on the interplay between the excluded volume effects, van der Waals attraction between monomers and its screening by the solvent [1]. The physics of the phase transition between these two states, the so-called globule-coil transition or θ -transition, is well captured by a simple lattice model of an interacting self-avoiding walk (ISAW), with an attractive interaction between monomers on the nearest neighboring sites of the lattice [2].

For magnetic polymers, where monomers carry magnetic moments (“spins”), the key parameter is the ratio of the relaxation times of magnetic and conformational degrees of freedom [3]: if spins are fast, conformations generate a quenched disorder for the magnetic subsystem [3–6]; in the opposite limit, the chain with quenched spins is qualitatively equivalent to a disordered copolymer; several models of this kind have been discussed in the literature [7–10].

The regime where both spins and conformations have comparable relaxation times has so far received much less attention. In this regime, spins are defined on a dynamic lattice, whose thermal fluctuations need to be taken into account self-consistently, on an equal footing with spin fluctuations. In this direction, Ref. [11] introduced a model where monomers of a SAW carry Ising spins, which interact via a short-range ferromagnetic interaction. The model is investigated on a three-dimensional (3D) cubic lattice using a mean-field approximation and Monte-Carlo (MC) simulations. In the absence of external magnetic field, Ref. [11] finds a first-order magnetic induced collapse transition—from a swollen paramagnetic phase to a ferromagnetic globular phase. (Upon increasing the magnetic field, the transition is reported to become continuous.) In Ref. [12] we considered a dynamic Hydrophobic-polar (HP) model in two dimensions (2D). The collapse transition was found to be consistent with a (continuous) θ -transition of a nonmagnetic ISAW.

In this paper, we consider a ferromagnetic Ising model

with spins placed on a self-avoiding walk (SAW) on a 2D square lattice. Using MC simulations, we also find a joint ferromagnetic and globule-coil transition, however our results indicate that it is continuous—unlike the 3D model, where it is first order [11]. We argue that the transition is characterized by the theta-point metric exponent ν , but the crossover exponent θ is markedly different. We also explore geometric properties of the model, and stress the role of the surface terms.

II. MODEL AND METHOD

We consider the model of Ref. [11]: Let \mathcal{U}_N be a set of all SAW conformations of N monomers joined by $N - 1$ links on a 2D square lattice. Each monomer i in a conformation $u \in \mathcal{U}_N$ carries an Ising spin, $s_i = \pm 1$, see Fig. 1. The spin-spin interaction is short-ranged: two spins interact if they are nearest neighbors on the lattice. Given a SAW conformation $u \in \mathcal{U}_N$ and a sequence of N spins, $\{s\}$, the Hamiltonian is

$$E(\{s\}, u) = -J \sum_{\langle i,j \rangle \in u} s_i s_j - h \sum_{j \in u} s_j. \quad (1)$$

Here the summation in the first term runs over pairs of spins, $i, j \in u$, which are nearest neighbors on the 2D lattice, and $J > 0$ is the ferromagnetic exchange coupling. In the second term, h is the magnetic field.

The partition function corresponding to Eq. (1) reads

$$Z = \sum_{u \in \mathcal{U}_N} \sum_{\{s\}} e^{-\beta E(\{s\}, u)}, \quad (2)$$

where $\beta = 1/kT$ is the inverse temperature. To set the energy units, we take $\beta = 1$ without loss of generality. Note that the summations in Eq. (2) run over both conformations and spin configurations.

For $h = J = 0$, spins decouple from conformations, and the model (1)-(2) reduces to a non-interacting SAW. In the limit $h \gg J$, all spins are aligned, and Eq. (1)-(2) reduces to the ISAW model. In this work we only consider the case $h = 0$. In the limit $J \ll 1$, the model (1)-(2)

describes Ising spins located on a non-interacting SAW— for the spins, the geometry is effectively one-dimensional and spontaneous magnetization is absent in the thermodynamic limit [3–5]. For $J \gg 1$, it is natural to expect a dense ferromagnetically ordered globule.

We note that since Eq. (1) only involves a single coupling constant, it is natural to expect that the ferromagnetic ordering sets in simultaneously with the globule-coil transition. In the next sections we verify this expectation and characterize the corresponding transition.

Method.— Most popular methods for Monte Carlo (MC) simulations of SAW-like model are based on chain growth techniques with pruning and enrichment [13], and their flat-histogram generalizations [14]. We use a different strategy: we work directly with fixed-length configurations and employ a variant of the worm algorithm [15] for interacting SAW-like models [16]. Specifically, the method uses two sets of MC updates. First is a bilocal reptation update, where we simultaneously remove a monomer from one end of a chain and add a monomer to the other end—the direction of the new edge and the value of the new spin are selected at random, see Fig. 1(a)-(b). This is nothing but the BEE move of Ref. [17]. Second, to render the reptation dynamics ergodic and improve convergence for dense configurations, we also use the “reconnect” update, where we rotate a single edge in the middle of the chain and attach it to the end of the chain—which needs to be adjacent to an internal monomer, see Fig. 1(a)-(c). The reconnect update is non-local since it reverses directions of $O(N)$ links of the SAW. However the Metropolis acceptance probability [18] equals unity since the update does not change the energy, Eq. (1). The reconnect update allows the simulation to escape from conformations where the end of the chain is trapped inside a dense configuration [16]. Furthermore, to improve convergence of magnetic observables, we also use standard Wolff cluster updates [19] for spins which keep the conformation fixed.

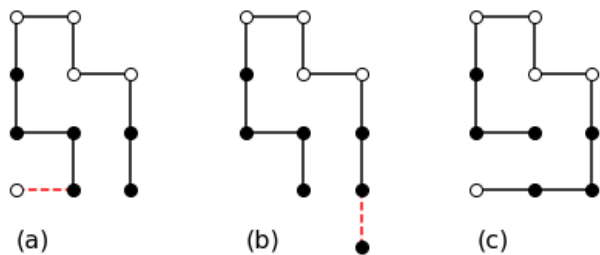


FIG. 1. Spin/SAW configurations and MC updates. Straight lines show a sample SAW, open circles denote spins-up, $s_j = +1$, and closed circles denote spins-down, $s_j = -1$. The BEE move is changing (a) to (b), where the edge shown in dashed red line in (a) is removed and the edge shown in dashed red line in (b) is added. The reconnect update is changing the configuration between (a) and (c). Note that configurations (a) and (c) have the same energy Eq. (1).

III. NUMERICAL SIMULATIONS

We simulate our model on a square 2D lattice for chains of up to $N = 10^4$ monomers. We typically use up to 10^9 MC updates for thermalization and collect statistics for 10^{10} to 10^{11} MC steps. Here in a single MC step we select an update (a BEE move, a reconnect or a spin cluster update) at random.

We perform simulations for $h = 0$ and $0 < J < 2$. We collect statistics for the mean energy, Eq. (1), per spin, $\epsilon = \langle E \rangle / N$, the mean magnetization per spin, $\langle m \rangle \equiv \langle \sum_{j \in u} s_j \rangle / N$ and its powers, $\langle m^2 \rangle$ and $\langle m^4 \rangle$. To characterize the structural properties of the model, we measure the mean end-to-end distance of the SAW, $\langle R_N^2 \rangle$. [20] Here and elsewhere in the text, angular brackets denote the MC average approximating the average over the Gibbs distribution (2).

Fig. 2(top) shows simulation results for mean square magnetization, $\langle m^2 \rangle$, as a function of J for several representative values of the SAW lengths N . At small values of J , $\langle m^2 \rangle \rightarrow 0$ at increasing N , which is consistent with the spontaneous magnetization being zero in the thermodynamic limit [3–5]. For larger values of the coupling constant, magnetization increases with increasing J and starts saturating for $J \gtrsim 0.88$, which suggests a ferromagnetic ordering for large J .

Fig. 2(bottom) illustrates the behavior of the mean energy, which approaches the asymptotic $N \rightarrow \infty$ value of $-2J$ for a densely packed fully magnetized walk. Finite-size corrections are clearly visible for both $\langle m^2 \rangle$ and $\langle \epsilon \rangle$, and we note that corrections are more pronounced for $J \gtrsim 0.82$, especially in Fig. 2(bottom).

Fig. 3 shows the dependence of the mean end-to-end distance, $\langle R_N^2 \rangle$, on N for several values of the coupling constant J . For $N \gg 1$ the scaling is visually consistent with a power-law,

$$\langle R_N^2 \rangle \sim N^{2\nu}(1 + \dots), \quad (3)$$

where dots represent corrections-to-scaling. For comparison, Fig. 3 also shows the asymptotic power laws $N^{2\nu}$ with $\nu = 3/4$ —which is a non-interacting SAW value (see e.g.,[21]),— and $\nu = 4/7$ —which is the exact value for the 2D ISAW at the θ -point [22].

Numerical data in Fig. 3 seem to indicate that the scaling of the end-to-end distance for our model crosses over from a non-interacting SAW limit for small J to a θ -point scaling for $J \sim 0.83$, and further on towards $\nu = 1/2$, which is expected for a dense globular phase. [23] Taken together, our numerical results shown in Figs. 2 and 3, indicate that both magnetic and structural properties of the model undergo a change at around $J \sim 0.83$.

The joint transition.—To locate the magnetic transition between paramagnetic and ferromagnetic phases, we compute the fourth-order Binder cumulant,

$$U_4 = 1 - \frac{\langle m^4 \rangle}{3\langle m^2 \rangle^2}, \quad (4)$$

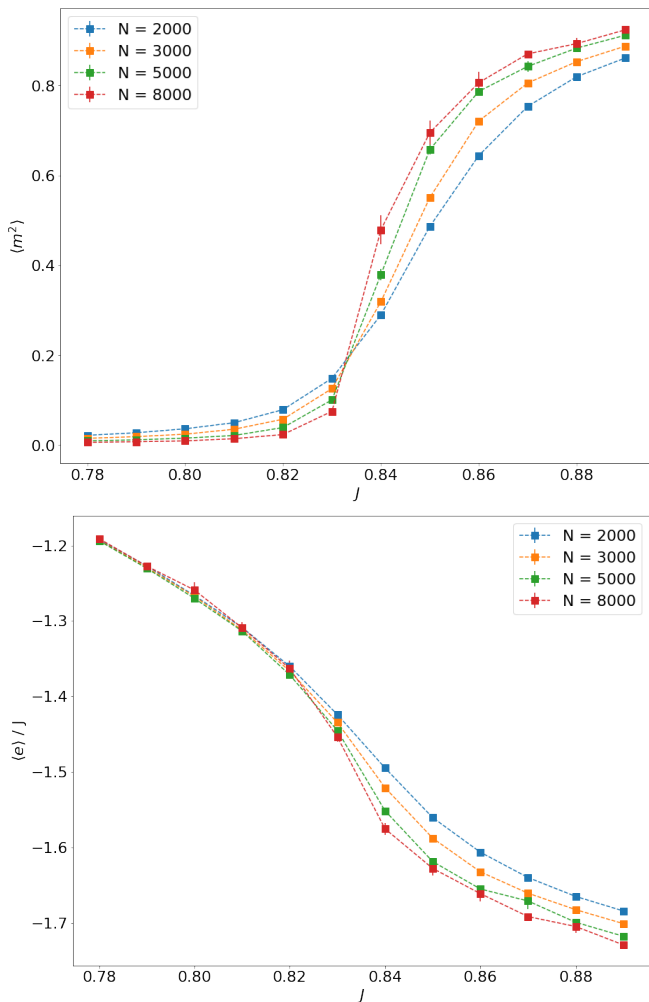


FIG. 2. (top) mean squared magnetization as a function of J for several values of N . Solid squares with errorbars are MC results, lines are to guide an eye only. Errorbars are estimated via binning analysis. In these simulations we use at least 7×10^9 MC steps per data point. (bottom) Mean energy as a function of J for several values of N . Squares are MC data with errorbars, and lines are to guide an eye. See text for discussion.

which is expected to become scale-independent at the transition [24].

Fig. 4(top) shows the dependence of the Binder cumulant (4) on interaction J for several values of N . For large values of the coupling constant (not shown in Fig. 4), U_4 tends to the value $2/3$ from below, as expected for a ferromagnetic state [24]. Curves of the cumulant U_4 for varying N cross around $J \approx 0.834$, indicative of the paramagnetic-to-ferromagnetic phase transition. Finite-size corrections are clearly visible in Fig. 4(top), thus to get a more precise estimate for the transition temperature, we analyze the pairwise crossings of the U_4 vs N curves for a series of N values from $N = 2000$ to $N = 9000$. The final estimate for the critical values is

$$J_c = 0.8340(5), \quad U_4^{(c)} = 0.308(8). \quad (5)$$

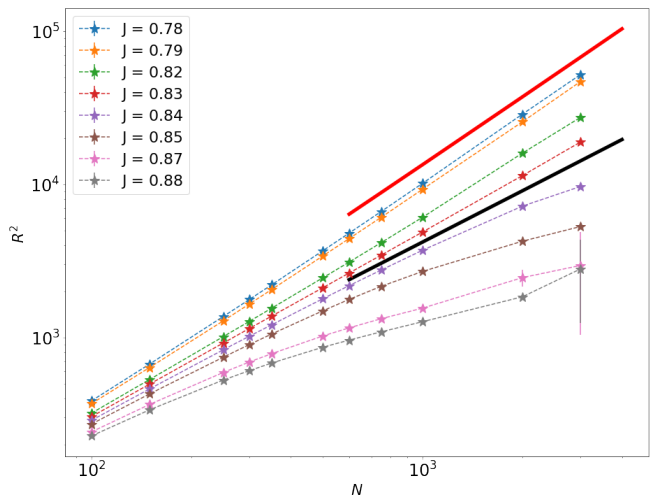


FIG. 3. Mean squared end-to-end distance as a function of N from $N = 100$ to $N = 3000$ for several values of J . Stars are MC data with errorbars, dashed lines are to guide an eye, and solid lines are $R^2 \sim N^{2\nu}$ with $\nu = 3/4$ (the solid red line) and $\nu = 4/7$ (the solid black line). See text for discussion.

This result (5) is close to, but distinct from the estimate $J_c = 1/1.18 \approx 0.847$, stated as preliminary without much discussion in Ref. [11].

Fig. 4(bottom) shows the dependence of the mean squared end-to-end distance (3). Here we rescale the values of R_N^2 by $N^{2\nu}$ with $\nu = 4/7$, as suggested by the analysis in the previous section. With this rescaling, $\langle R^2 \rangle / N^{2\nu}$ becomes N -independent (modulo corrections-to-scaling) at $J_\theta = 0.833(1)$ which is consistent with Eq. (5) within the combined errorbars.

We also checked that the existence of the crossing is sensitive to the value of the metric exponent ν : if ν is changed by more than 0.07, the crossing disappears.

We thus conclude that our numerical data suggest that (i) the ferromagnetic and globule-coil transition occur simultaneously at the critical coupling constant given by Eq. (5), and (ii) the scaling of the end-to-end distance at the transition is consistent with the θ -point metric exponent $\nu = 4/7$.

The crossover exponent.—We turn our attention to estimating the crossover exponent ϕ which quantifies the deviation from criticality via the scaled coupling $x = (J - J_c)/N^{-\phi}$ [21]. Specifically, the end-to-end distance is expected to follow $\langle R_N^2 \rangle = N^{2\nu} f(x)$ where $f(\cdot)$ is a dimensionless function of a dimensionless variable. To probe this Ansatz, we perform data collapse of the end-to-end distance, where we keep $\nu = 4/7$ fixed at its theta-point value [22], and vary J_c and ϕ . This procedure is illustrated in Fig. 5.

We find that our MC data are consistent with $J_c = 0.833(1)$ and $\phi = 0.7(1)$, where the errorbars are conservative estimates from visual inspection of the quality of the data collapse. We note that the value of J_c is consistent with Eq. (5). The crossover exponent clearly

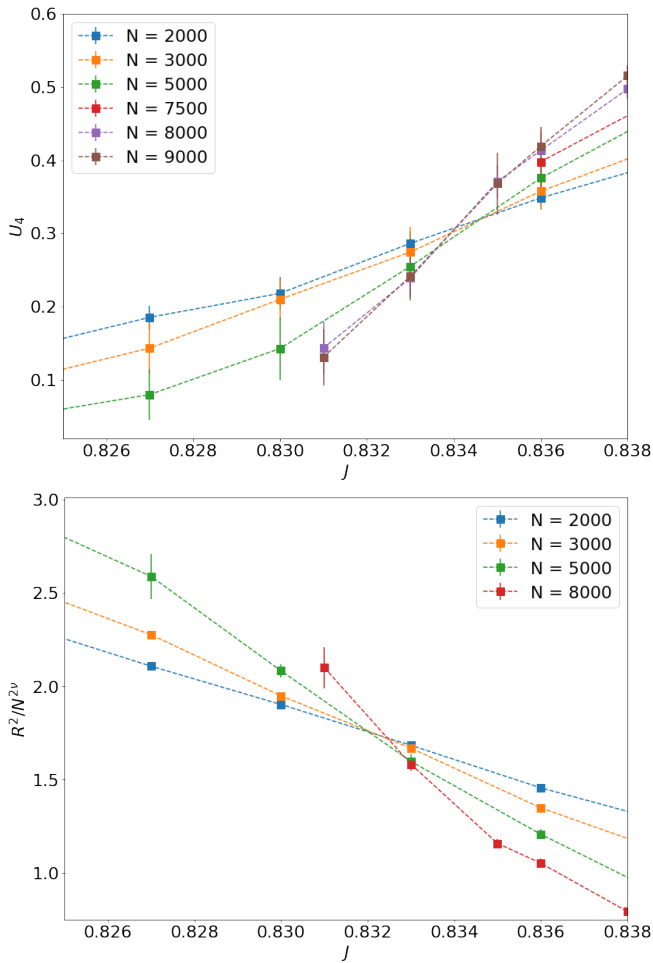


FIG. 4. (top) Binder cumulants (4) as a function of J for several values of N . Solid squares with errorbars are MC results, lines are to guide an eye only. Errorbars are estimated via a Gaussian resampling from errorbars of $\langle m^4 \rangle$ and $\langle m^2 \rangle$. (bottom) Scaled mean end-to-end distance (3) with $\nu = 4/7$, which is the exact value for the 2D ISAW at the θ -point [22]. Squares are MC data with errorbars, and lines are to guide an eye. See text for discussion.

differs from the θ -point value for the ISAW model, where the Coulomb gas prediction is $\phi = 3/7$ [22] and numerical estimates are somewhat larger (see Ref. [25] and the discussion therein).

We also perform a similar data collapse analysis for the magnetization, where the scaling Ansatz is $\langle m^2 \rangle = N^{-2\beta\phi} g(x)$, where $g(x)$ is a scaling function and β is the order parameter exponent. Fig. 6 illustrates the procedure where we take $\beta = 1/8$ —which is the value for the 2D Ising universality class. While the quality of our numerical data does not allow for estimating critical exponents with accuracy of any less than, say, 50%, we find that our data are consistent with the order parameter exponent taking the 2D Ising value, and the crossover exponent $\phi \approx 0.7$.

We stipulate that a high-precision estimate of the

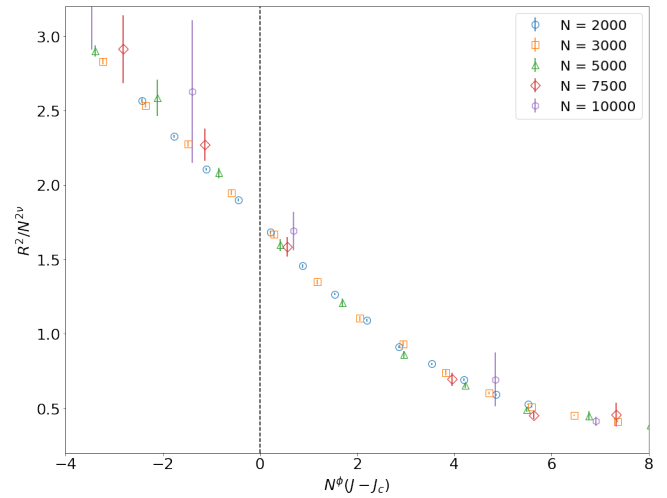


FIG. 5. Data collapse for the scaled end-to-end distance, $\langle R_N^2 \rangle / N^{2\nu}$, vs the scaled coupling $x = (J - J_c)N^\phi$. We fix $\nu = 4/7$ and vary J_c and ϕ . On this plot, $J_c = 0.832$ and $\phi = 0.7$. From visual inspection of the quality of the collapse, we estimate $J_c = 0.833(1)$ and $\phi = 0.7(1)$. See text for discussion.

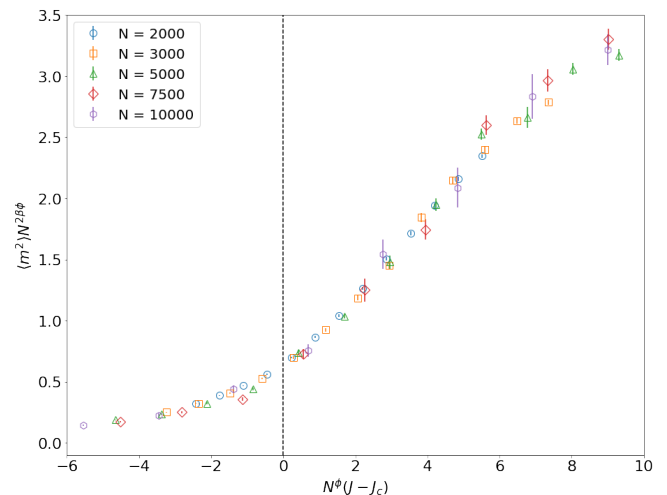


FIG. 6. Data collapse for the second moment of magnetization $\langle m^2 \rangle$. In this plot we use $\phi = 0.71$, $J_c = 0.832$ and $\beta = 1/8$. See text for discussion.

crossover exponent and/or the order parameter exponent should take into account two sources of corrections. First, for a disordered Ising model, logarithmic corrections [26], are known to lead to apparently varying exponents [27]. Second, non-universal corrections due to the surface tension are strong for 2D SAWs [28] because the surface-to-volume ratio in 2D scales as $\sim N^{-1/2}$ which is close to the universal θ -point values $\nu = 4/7$ and $\phi = 3/7$.

Bulk to surface ratio.— Strictly speaking, the very notions of bulk and surface are not well defined for $J < J_c$, where typical conformations are coil-like. To come up with a quantitative characteristic which is meaningful

across the globule-coil transition and can be interpreted as a bulk-to-surface ratio in the globular phase, we consider a local neighborhood of a monomer. We note that each monomer (apart from two endpoints of the chain) can be classified according to the number of its neighbor monomers as being either 1D-like (two neighbors), 2D-like (four neighbors) or surface-like (3 neighbors).

For a length- N conformation, we count the numbers of monomers of each kind; dividing by N we obtain the fractions, n_α ($\alpha = 2, 3, 4$), so that $n_2 + n_3 + n_4 = 1 - 2/N$. Qualitatively, the ratio $n_2/(n_3 + n_4)$ characterizes a blob-and-link structure of a coil-type conformation, and n_4/n_3 can be interpreted as a proxy for a bulk-to-surface ratio.

Fig. 7 shows the fractions of each kind of monomers as a function of J for chains of length $N = 1000$ to 4900. For comparison, we also compute the corresponding fractions for an ISAW model (i.e., Eqs. (1)-(2) with $h \gg J$).

Several features stand out in Fig. 7. First, even in the non-interacting SAW limit, $J \rightarrow 0$, conformations are not fully 1D-like, as $n_2 \approx 0.75$ only (the finite-size corrections become negligible for $N \gtrsim 100$). The “bulk” fraction, n_4 , is vanishingly small in the $J \rightarrow 0$ regime, and the fraction of the “surface” monomers, n_3 , tends to 0.25 for $J \rightarrow 0$. In the opposite limit of large J , the 1D-like fraction tends to zero and the “bulk” fraction grows. Most surprisingly, the “surface” fraction, n_3 , develops a peak for both ISAW and Ising models in the vicinity of their respective collapse transitions.

While the relation between these results to a bulk/surface ratio of real polymer chains is qualitative at best, and that more work is needed to understand the nature of the peaks of $n_3(J)$, these results do illustrate the importance of surface effects and stress the qualitative difference between the magnetic SAW models and spin networks with mixed 1D / 2D local connectivity [29].

Relation to the Ising model on rectangular lattices.—

It is instructive to compare the critical value of the Binder cumulant, $U_4^{(c)}$, Eq. (5), to the values for a usual Ising model on a regular grid. For the Ising model on a rectangular $L \times W$ lattice, the critical value of U_4 depends on the boundary conditions and on the aspect ratio of the lattice, L/W [30, 31]. The dependence on the boundary conditions is strong: on an $L \times L$ lattice with periodic boundary conditions, $U^{(c)} \approx 0.61$, while open boundary conditions lead to $U^{(c)} \approx 0.4$. Furthermore, on the lattice with open boundary conditions, $U^{(c)}$ decreases continuously for increasing aspect ratio L/W down to ≈ 0.35 for $L/W = 2$ [31] and further down for larger aspect ratios.

The critical value $U_4^{(c)}$, Eq. (5), is approximately compatible with the result for the Ising model on a rectangular lattice with open boundary conditions and the aspect ratio given by the ratio of the eigenvalues of the gyration tensor of an interacting SAW at the θ -point [25]. More work is needed to accurately trace this connection.

The nature of the transition.— In 3D, the transition is clearly first-order [11]. Our simulations indicate that the transition is continuous in 2D. First of all, the Binder cumulant (4) is a monotonic function of J for fixed N ,

cf Fig. 4(top). This is consistent with a continuous transition, and is in contrast to the expected behavior for a first-order transition, where the cumulant is non-monotonic and develops a dip at J_c as N increases [32].

We then perform simulations for the specific heat capacity per monomer, which is given by the second moment of the energy, Eq. (1)-(2),

$$C = \frac{1}{N} (\langle E^2 \rangle - \langle E \rangle^2) \quad (6)$$

For finite values of N , the heat capacity is expected to have a peak in the critical region. The peak can be rounded and shifted by finite-size corrections, and the evolution of the peak height and shape is expected to be very different for first-order and continuous transitions: For a first order transition, the height of the peak of $C(J)$ is expected to be linear in N , while the width is expected to shrink as $\sim N^{-1}$ [32]. For continuous transitions, the structure of $C(J)$ in the vicinity of J_c is controlled by the heat capacity exponent α , which is typically different from unity.

Fig. 8 shows our numerical results for the specific heat capacity. We note that numerical cancellations in Eq. (6) magnify statistical errors of MC simulations, thus limiting the values of N accessible in these simulations to be about an order of magnitude smaller than those in Figs. 2-6—which is comparable to the values reported in Ref. [11]. At these values of $N \leq 500$, shown in Fig. 8, finite-size corrections are very strong. Nevertheless, the available numerical data suggest that the peak height dependence on N is sublinear and the peak widths shrinks slower than $1/N$. The overall shape of $C(J)$ curves in Fig. 8 is drastically different from those observed for a first-order transition in 3D in Ref. [11]. We interpret these observations, however limited, as an additional indication of a transition being continuous, with the heat capacity exponent $\alpha < 1$.

We also note that we observe a single peak of $C(J)$, not a two-peak structure reported for a site-diluted Ising model [33] and a network of Ising spins with mixed 1D/2D local connectivity [29]. The difference with the latter is not surprising given the role of the surface-like spins, cf Fig. 7.

To further check the nature of the transition, we compute distributions of observables. Fig. 9 shows the distribution of the magnetization for $N = 10^4$ in the vicinity of the transition, Eq. (5). The distribution is Gaussian-like on the paramagnetic side, $J < J_c$, broadens on approach to the critical coupling, and develops a clear ferromagnetic structure ($m = \pm 1$) for $J > J_c$. In the critical region, we see no signs of a phase coexistence which would signal a first-order transition.

IV. CONCLUSIONS AND OUTLOOK

Concluding, we study a 2D model of a magnetic polymer chain where monomers of a self-avoiding walk on a

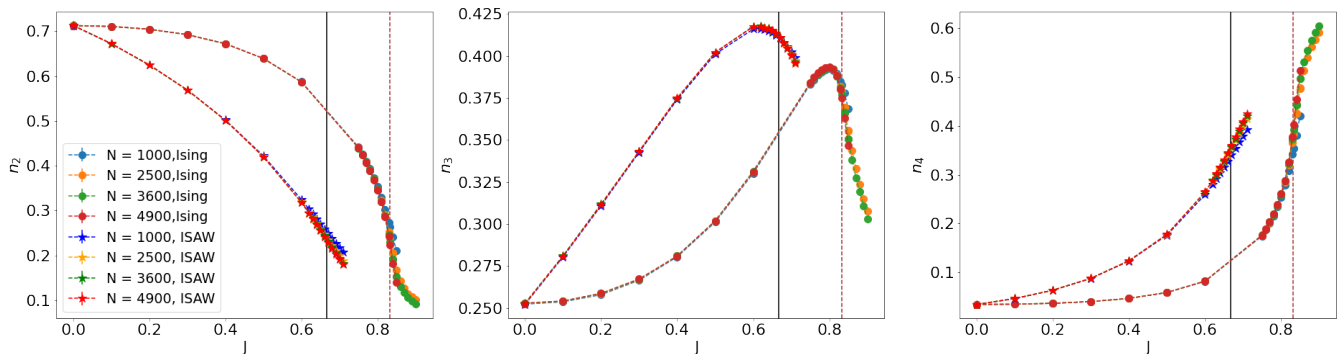


FIG. 7. Fractions of monomers with two neighbors, n_2 , (left), three neighbors, n_3 , (center) and four neighbors, n_4 , (right). Solid circles are the MC data for the Ising model (1)-(2), stars are the MC data for the ISAW model, and dotted lines are to guide an eye. The vertical solid black line is the theta-point for the ISAW, taken from Ref.[25]. The vertical dashed brown line is Eq. (5).

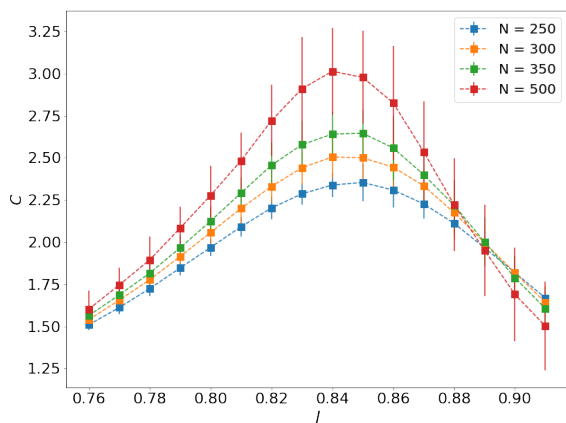


FIG. 8. The specific heat capacity per monomer, Eq. (6), as a function of the coupling constant J . Errorbars are estimated via statistical resampling from MC data for the first and second moments of the energy. See text for discussion.

lattice carry Ising spins [11]. We use a variant of the worm algorithm to simulate fixed-length chains of up to 10^4 monomers. We find a joint transition—where both spins order ferromagnetically and the SAW collapses into a globular phase—at $J/T = 0.8340(5)$. The very fact that the transitions occur simultaneously can be traced to the specifics of the model, which only has a single coupling constant, the exchange integral for the short-range spin-spin interaction. What is less clear *a priori*, is the nature of the transition. Our results suggest that the transition is continuous, in contrast to a similar 3D model, where it is reported to be first-order [11]. Our numerical results suggest that some critical exponents (but not all of them) are inherited from the “parent” models, namely the θ -polymer ISAW model, and the Ising model. Specifically, we present numerical evidence that the metric exponent ν at the transition takes the θ -point value

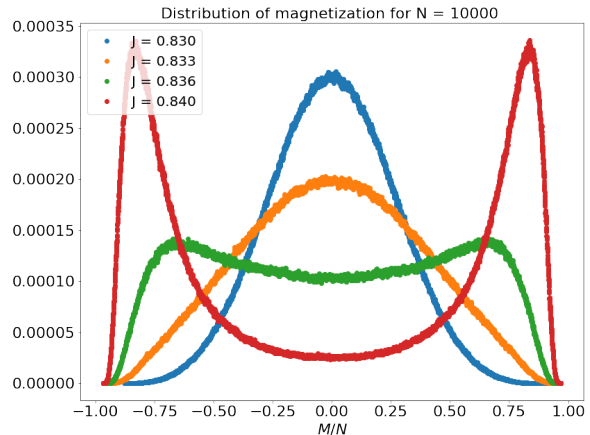


FIG. 9. Distribution of the magnetization $m = \sum_{j \in U} s_j / N$ for $N = 10000$. The coupling constants are $J = 0.830 < J_c$ (blue points), $J = 0.833 \approx J_c$ (orange), $J = 0.836$ (just above the J_c , green), and $J = 0.840 > J_c$ (red). Each simulation uses $\sim 7 \times 10^9$ MC steps.

$\nu = 4/7$, but the crossover exponent $\phi \approx 0.7$, which is clearly different from the θ -polymer value of $3/7$. We also present indications that the magnetic order parameter exponent β is consistent with the 2D Ising universality class value $\beta = 1/8$, however the accuracy of this observation given our simulation results is relatively weak.

We study geometric properties of the model and classify the local connectivity of monomers of the chain into 1D-like, bulk-like and surface-like. A possible interpretation of our numerical results is that the surface-to-bulk ratio has a peak in the vicinity of the transition. Incidentally, we also find numerical evidence that for a non-interacting SAW, the fraction of 1D-like monomers is $1/4$ in the thermodynamic limit. To the best of our knowledge, this was previously not discussed in the literature. More work is needed to clarify the status and physical

meaning of these numerical results.

Concerning future work, it would be interesting to explore more realistic models of magnetic polymers, e.g. by considering Potts or Heisenberg type models and general dipole-dipole couplings in two and three dimensions. Models with separate coupling constants might generate richer phase diagrams with separate globule-coil and magnetic transitions.

Possible experimental realizations of magnetic polymers, for which our model and its suggested generalizations may be applicable, include magnetic filaments where magnetic nanoparticles are either cross-linked by a polymer to form linear structures—these can be realized via e.g. biotemplating [34]—or self-organize into one-dimensional like structures at liquid-liquid interfaces [35]. Monte Carlo simulations of models of magnetic polymers may complement molecular dynamics studies of magnetic

filaments [36].

When this work was completed, we became aware of an independent study of the same model in Ref. [37]. Our estimates of the location of the transition and critical exponents and those of Ref. [37] are consistent within the combined errorbars.

V. ACKNOWLEDGMENTS

We acknowledge financial support by RFBR according to the research project No 19-07-01117. K.F. and I.P. acknowledge support within the Project Teams framework of MIEM HSE. Numerical simulations were performed using the computational resources of HPC facilities at HSE University [38]. Multiple illuminating discussions with Lev Shchur and Yuri Budkov are gratefully acknowledged.

-
- [1] P-G de Gennes. *Scaling concepts in polymer physics*. Cornell University Press, 1979.
- [2] C. Vanderzande. *Lattice models of polymers*. Cambridge University Press, 1998.
- [3] M. Aerstens and C. Vanderzande. Ising model on a SAW. *J. Phys. A: Math. Gen.*, 25:735, 1992.
- [4] B. K. Chakrabarti and S. Bhattacharya. Study of an Ising model on a self-avoiding walk lattice. *J. Phys. C: Solid State Physics*, 16:L1025, 1983.
- [5] B. K. Chakrabarti and S. Bhattacharya. A real-space renormalization group study of the Ising model on self-avoiding walk chains. *J. Phys. A: Math. Gen.*, 18:1037, 1985.
- [6] A. Papale and A. Rosa. The Ising model in swollen vs. compact polymers: Mean-field approach and computer simulations. *Eur. Phys. J. E*, 41, 12 2018.
- [7] G. Z. Archontis and E. I. Shakhnovich. Phase transitions in heteropolymers with “secondary structure”. *Phys. Rev. E*, 49:3109, 1994.
- [8] A. R. Khokhlov and P. G. Khalatur. Protein-like copolymers: computer simulation. *Physica A*, 249(1):253–261, 1998.
- [9] H.K. Murnen, A.R.Khokhlov, P.G. Khalatur, R.A. Segalman, and R.N. Zuckermann. Impact of hydrophobic sequence patterning on the coil-to-globule transition of protein-like polymers. *Macromolecules*, 45(12):5229–5236, 2012.
- [10] V. Blavatska and W. Janke. Conformational transitions in random heteropolymer models. *J. Chem. Phys.*, 140:034904, 2014.
- [11] T. Garel, H. Orland, and E. Orlandini. Phase diagram of magnetic polymers. *Eur. Phys. J. B*, 12:261–268, 1999.
- [12] K. Faizullina and E. Burovski. Globule-coil transition in the dynamic HP model. *J. Phys.: Conf. Ser.*, 1740:012014, 1 2021.
- [13] P. Grassberger. Pruned-enriched Rosenbluth method: Simulations of θ polymers of chain length up to 1 000 000. *Phys. Rev. E*, 56:3682–3693, Sep 1997.
- [14] T. Prellberg and J. Krawczyk. Flat histogram version of the pruned and enriched Rosenbluth method. *Phys. Rev. Lett.*, 92:120602, Mar 2004.
- [15] N. Prokof’ev and B. Svistunov. Worm algorithms for classical statistical models. *Phys. Rev. Lett.*, 87:160601, Sep 2001.
- [16] N. Prokof’ev E. Burovski and B. Svistunov. unpublished, 2002.
- [17] S. Caracciolo, M. Papinutto, and A. Pelissetto. Dynamic critical behavior of an extended reptation dynamics for self-avoiding walks. *Phys. Rev. E*, 65:031106, Feb 2002.
- [18] N. Metropolis, A.W. Rosenbluth, M.N. Rosenbluth, A.H. Teller, and Teller.E. Equation of state calculations by fast computing machines. *J. Chem. Phys.*, 21(6):1087–1092, 1953.
- [19] U. Wolff. Collective Monte Carlo updating for spin systems. *Phys. Rev. Lett.*, 62:361–364, Jan 1989.
- [20] In the literature, the gyration radius is often considered instead; however the asymptotic properties of the radius of gyration and end-to-end distance are expected to be the same (see, e.g. [17]), and the latter is simpler to work with numerically.
- [21] E.J.J.v. Rensburg. *The Statistical Mechanics of Interacting Walks, Polygons, Animals and Vesicles*. Oxford Lecture Series in Mathe. Oxford University Press, 2015.
- [22] B. Duplantier and H. Saleur. Exact tricritical exponents for polymers at the theta point in two dimensions. *Phys. Rev. Lett.*, 59:539, 1987.
- [23] Following Ref. [39], we also fit the data shown in Fig. 3 with a four-parameter model, $\log(R_N^2 + k_1) = 2\nu \log(N + k_2) + b$, with fit parameters ν , b , k_1 and k_2 . Here b , k_1 and k_2 are phenomenological parameters meant to mimic corrections to scaling. While this model is not expected to be fully accurate—it misrepresents corrections-to-scaling exponents and thus produces wrong results for ν close to the globular phase—it does support the expectation from a visual inspection of Fig. 3 that the metric exponent ν agrees with the θ -point value $\nu = 4/7$ around $J \approx 0.83$.
- [24] K. Binder. Finite size scaling analysis of Ising model block distribution functions. *Z. Phys. B*, 43:119, 1981.
- [25] S. Caracciolo, M Gherardi, M. Papinutto, and A. Pelissetto. Geometrical properties of two-dimensional inter-

- acting self-avoiding walks at the θ -point. *J. Phys. A: Math. Theor.*, 44(11):1–24, 2011.
- [26] V. S. Dotsenko and V. S. Dotsenko. Critical behaviour of the phase transition in the 2D Ising model with impurities. *Adv. Phys.*, 32:129, 1983.
- [27] H. G. Ballesteros, L.A. Fernandez, V. Martín-Mayor, A.M. Sudupe, G. Parisi, and J.J. Ruiz-Lorenzo. Ising exponents in the two-dimensional site-diluted Ising model. *J. Phys. A: Math. Gen.*, 30:8379, 1997.
- [28] P. Grassberger and R. Hegger. Simulations of θ -polymers in 2 dimensions. *Journal de Physique I*, 5(5):597–606, 1995.
- [29] O.T. Valls A.N. Malmi-Kakkada and C. Dasgupta. Ising model on a random network with annealed or quenched disorder. *Phys. Rev. B*, 90:024202, Jul 2014.
- [30] W. Selke and L. N. Shchur. Critical Binder cumulant in two-dimensional anisotropic Ising models. *J. Phys. A: Math. Gen.*, 38(44):L739–L744, oct 2005.
- [31] W. Selke. Critical Binder cumulant of two-dimensional Ising models. *Eur. Phys. J. B*, 51(2):223–228, 2006.
- [32] K. Binder and D.P. Landau. Finite-size scaling at first-order transitions. *Phys. Rev. B*, 30:1477, 1984.
- [33] W. Selke, L.N. Shchur, and O.A. Vasiliev. Specific heat of two-dimensional diluted magnets. *Physica A*, 259:338, 1998.
- [34] F. Vonderviszt E.Bereczk-Tompa, B. Horvath, I. Szalaid, and M. Posfai. Biotemplated synthesis of magnetic filaments. *Nanoscale*, 9:15062, 2017.
- [35] J.J. Benkoski, S.E. Bowles, R.L. Jones, J.F. Douglas, J. Pyun, and A. Karim. Self-assembly of polymer-coated ferromagnetic nanoparticles into mesoscopic polymer chains. *J. Polym. Sci., Part B: Polym. Phys.*, 46:2267, 2008.
- [36] D. Mostarac, P.A. Sanches, and S. Kantorovich. Characterisation of the magnetic response of nanoscale magnetic filaments in applied fields. *Nanoscale*, 12:13933–13947, 2020.
- [37] D.P. Foster and D. Majumdar. Critical behavior of magnetic polymers in two and three dimensions. *Phys. Rev. E*, 104:024122, Aug 2021.
- [38] P. S. Kostenetskiy, R. A. Chulkevich, and V. I. Kozyrev. HPC resources of the Higher School of Economics. *J. Phys.: Conf. Ser.*, 1740:012050, jan 2021.
- [39] A. Berretti and A.D. Sokal. New Monte Carlo method for the self-avoiding walk. *Journal of Statistical Physics*, 40(3-4):483–531, 1985.